

Phosphite Bearing $[(\mu\text{-ADT})^R\text{Fe}_2(\text{CO})_6]$ (ADT = Azadithiolate) Moieties: A Tool for the Building of Multimetallic $[\text{FeFe}]$ -Hydrogenase Mimics

Alejandro Torres, Diego J. Vicent, Alba Collado, Mar Gómez-Gallego, Carmen Ramírez de Arellano, and Miguel A. Sierra*



Cite This: *Organometallics* 2023, 42, 316–326



Read Online

ACCESS |



Metrics & More

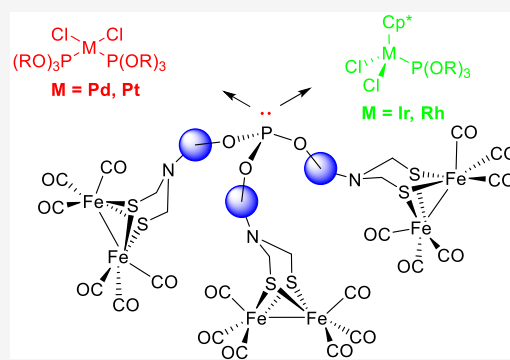


Article Recommendations



Supporting Information

ABSTRACT: A new phosphite ligand having three $[(\mu\text{-ADT})^R\text{Fe}_2(\text{CO})_6]$ ($R = p\text{-HOC}_6\text{H}_4$) moieties (**2**) has been prepared in good yield by the reaction of complex $[(\mu\text{-ADT})^R\text{Fe}_2(\text{CO})_6]$ ($R = p\text{-HOC}_6\text{H}_4$) **1a** with PCl_3 . Coordination of this phosphite to $[\text{PdCl}_2(\text{MeCN})_2]$ or $[\text{PtCl}_2(\text{DMSO})_2]$ forms heterometallic square planar complexes **5** ($\text{C}_{84}\text{H}_{48}\text{Cl}_2\text{Fe}_{12}\text{N}_6\text{O}_{42}\text{P}_2\text{MS}_{12}$) ($M = \text{Pt}, \text{Pd}$) in excellent yields. Three-legged piano stool complexes **6** ($\text{C}_{52}\text{H}_{39}\text{Cl}_2\text{Fe}_6\text{N}_3\text{O}_{21}\text{PMS}_6$) ($M = \text{Rh}, \text{Ir}$) were obtained by the reaction of phosphite **2** with $[\text{MCl}_2\text{Cp}^*]_2$ ($M = \text{Rh}, \text{Ir}$) in good yields. The formation of complexes **5** and **6** demonstrates the versatility of this new ligand for forming different heteropolymetallic complexes under mild reaction conditions. Moreover, the open-chain derivatives $[(\mu\text{-ADT})^R\text{Fe}_2(\text{CO})_6]$ ($R = \text{HOCH}_2\text{CH}_2$, $o\text{-HOC}_6\text{H}_4$) (**1b** and **1c**, respectively) form cyclic complexes **4** by spontaneous intramolecular CO substitution by the P atom in one of the three $[\text{FeFe}]$ fragments. The electrocatalytic behavior of complexes **2** and **4** upon the addition of AcOH is similar to that of related $[(\mu\text{-ADT})\text{Fe}_2(\text{CO})_6]$ derivatives. The successive additions of AcOH cause an increase in the current intensity in the wave at about -1.80 V for heteropolymetallic complexes **5** and **6**. However, the appearance of a new wave around -1.40 V in complexes **5** points to an acid-promoted side reaction in the electrochemical process.



INTRODUCTION

Hydrogenases are metalloenzymes that catalyze the reversible conversion of H^+ to H_2 .^{1–7} Depending on the metal center present in their active sites, they are classified into three types: $[\text{FeFe}]$ -hydrogenases, $[\text{NiFe}]$ -hydrogenases, and $[\text{Fe}]$ -hydrogenases (Figure 1). In particular, $[\text{FeFe}]$ -hydrogenases are the most efficient in H_2 production.^{1,7} For this reason, in the last 20 years, enormous efforts have been devoted to understanding the hydrogen evolution reaction (HER) promoted by these enzymes.⁸ To overcome the limitations encountered during the use of hydrogenases in the bulk production of H_2 , especially their thermal instability and their high sensibility to

oxygen, the attention of researchers has been directed to the preparation of simple molecules able to mimic the action of the enzymes. In this context, a myriad of complexes based on diiron hexacarbonyl organometallic structures ($[(\mu\text{-SR})_2\text{Fe}_2(\text{CO})_6]$) have been synthesized and studied.^{9–15} These complexes are generally known as $[\text{FeFe}]$ -hydrogenase mimics.

An interesting approach to fulfilling the requirements for functional hydrogenase mimics consists of the incorporation of anchoring points in their structures capable of binding to other metal centers. Well-known are those mimics bearing pyridine, bipyridine, or terpyridine moieties,^{16–19} which are able to coordinate Ru complexes that can act as photosensitizers. Several Ru complexes are used as efficient photocatalysts to produce H_2 from diverse $[\text{FeFe}]$ -hydrogenase mimics, although the process needs two equivalents of sacrificial

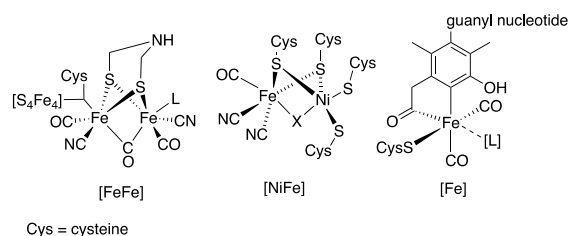
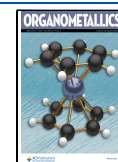


Figure 1. Schematic representation of the three types of hydrogenases.

Received: November 10, 2022

Published: February 15, 2023



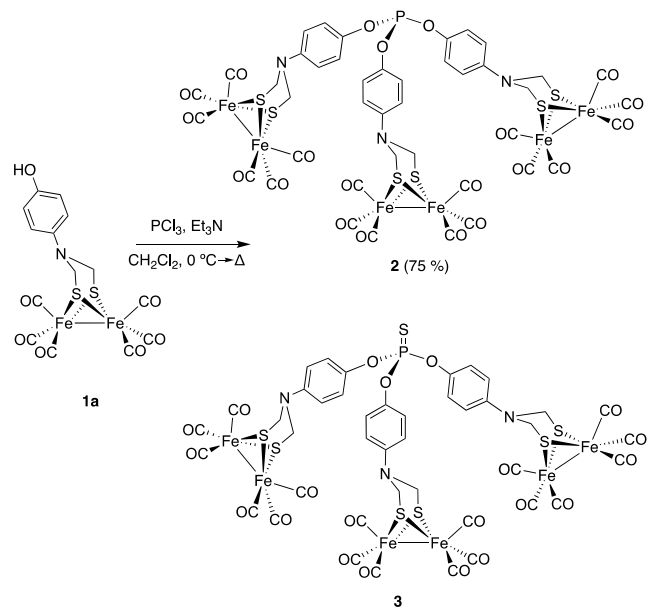
oxidants (usually ascorbic acid or ascorbates) for each molecule of H_2 produced.^{20,21} Additionally, $[(\mu\text{-SR})_2\text{Fe}_2(\text{CO})_6]$ fragments have been incorporated into peptide platforms,^{22–27} CdSe quantum dots,²⁸ polymer supports,^{29,30} MOFs,^{31,32} Si surfaces,^{33–35} and others.¹³

In this context, we devised the incorporation of phosphite groups in the $[\text{FeFe}]$ structure as a strategy to add an anchoring point to the $[\text{FeFe}]$ mimic suitable to coordinate to diverse metal centers and surfaces. Phosphite groups have been widely employed as ligands of the Fe centers of $[\text{FeFe}]$ -hydrogenase mimics^{36–44} to modify the electronic properties of the metal or to study the mechanism of the HER.⁴⁵ Nevertheless, to the best of our knowledge, the use of a phosphite group to coordinate $[\text{FeFe}]$ -hydrogenase mimics to metal centers has not been described. Herein, we report the synthesis and electrochemical characterization of the first $[\text{FeFe}]$ -hydrogenase mimics bearing a phosphite moiety capable of coordinating to metal centers, as well as the self-displacement of one CO ligand in the tris- $[\text{FeFe}]$ compound and the preparation of square-planar Pd and Pt complexes and half-sandwich Ir and Rh complexes. The electrocatalytic properties of these compounds will be presented.

RESULTS AND DISCUSSION

Complex **1a** was prepared following literature procedures⁴⁶ and reacted with PCl_3 in boiling CH_2Cl_2 in the presence of Et_3N (Scheme 1). The $^{31}\text{P}\{^1\text{H}\}$ NMR analysis of the reaction

Scheme 1. Preparation of Complexes **2** and **3**

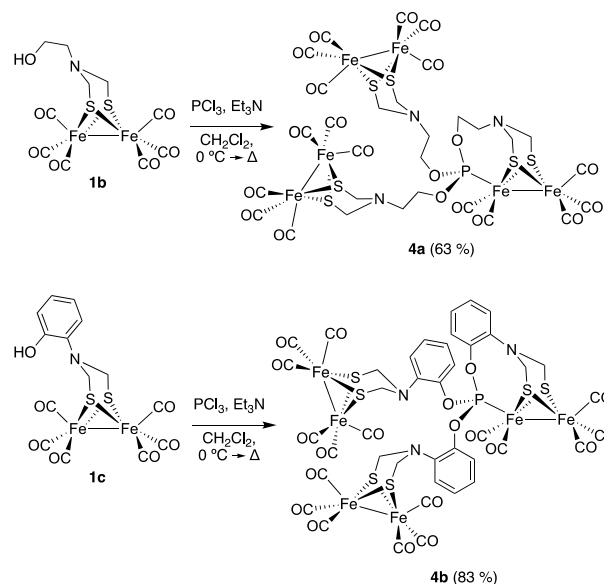


mixture showed two different signals: one at 128.59 ppm, which corresponds to the chemical shift of the desired compound, phosphite **2**; and another one at 54.81 ppm, which agrees with the corresponding thiophosphate (**3**).⁴⁷ The products were separated by column chromatography in neutral Al_2O_3 . The major compound **2** was isolated in a 75% yield. The minor product, thiophosphate **3**, was probably generated by the thio-oxidation of the free phosphite (**2**) in the presence of elemental sulfur (produced by the thermal decomposition of the starting material) or by nucleophilic substitution on a thiol from the bridging ADT ligand.⁴⁸

The structure of thiophosphate complex **3** was unambiguously demonstrated by its independent synthesis. Thus, 3 equiv of compound **1a** was reacted with PSCl_3 in the presence of Et_3N in CH_2Cl_2 at 65 °C using a microwave reactor. The compound thus obtained (**3**, 43% yield) was identical to the compound obtained in the reaction depicted in Scheme 1.

Aromatic ADT ligands bearing the OH group in the *ortho*-position of a phenyl group (**1c**) or an aliphatic alcohol (**1b**) led to a different reaction outcome. Complex $[(\mu\text{-ADT})^R\text{Fe}_2(\text{CO})_6]$ ($R = \text{CH}_2\text{CH}_2\text{OH}$) (**1b**), derived from ethanolamine, was prepared following literature procedures⁴⁹ and reacted with PCl_3 in boiling CH_2Cl_2 in the presence of Et_3N (Scheme 2). Phosphite **4a** having a P atom coordinated

Scheme 2. Preparation of Complexes **4a** and **4b**



to one of the three $[\text{FeFe}]$ centers was isolated in a 63% yield (Scheme 2). The intramolecular coordination of ligands containing phosphorus functionalities to $[(\mu\text{-SR})_2\text{Fe}_2(\text{CO})_6]$ has been reported in the literature.^{43,50} A similar result was obtained from complex **1c** derived from *o*-aminophenol. This complex also reacted cleanly with PCl_3 to yield complex **4b** (83% isolated yield). Acyclic phosphites similar to **2** were not detected in any of these reactions.

Complexes **4a** and **4b** were fully characterized by NMR and FTIR spectroscopy and mass spectrometry. The $^{13}\text{C}\{^1\text{H}\}$ NMR spectra of compounds **4** show three signals corresponding to CO ligands. The coordination of the P atom to one of the Fe centers was supported by the presence of a doublet at 211.5 ppm ($J_{\text{C-P}} = 13.0$ Hz) for **4a** and one at 209.7 ppm ($J_{\text{C-P}} = 7.0$ Hz) for **4b**. These signals correspond to the C atoms of CO ligands coupled with the P atom. Additionally, a phosphorus signal corresponding to a phosphite moiety coordinated to a Fe atom was found at 186.78 ppm for **4a** and at 175.91 ppm for **4b** in their $^{31}\text{P}\{^1\text{H}\}$ NMR spectra.^{51,52} The structure of compound **4a** was determined by single-crystal X-ray diffraction analysis (Figure 2).

The structure shows a phosphite ligand bridging three $[(\mu\text{-SR})_2\text{Fe}_2]$ units with two $[(\mu\text{-SR})_2\text{Fe}_2(\text{CO})_6]$ moieties bonded through the phosphite P–O bond in a terminal mode and a cyclometalated $[(\mu\text{-SR})_2\text{Fe}_2(\text{CO})_5]$ unit chelated through the phosphite P–O bond and the phosphorus atom. Thus, the

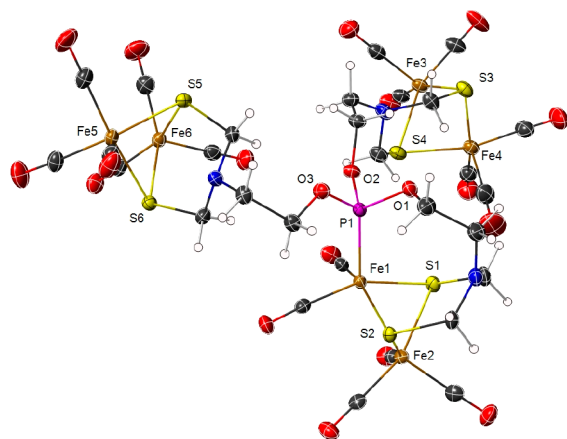


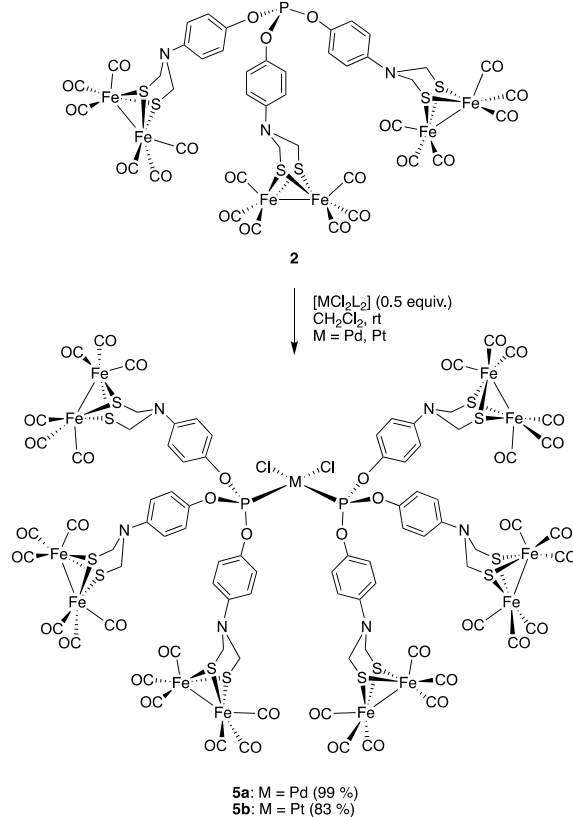
Figure 2. X-ray thermal ellipsoid plot of **4a** (50% probability level) with the labeling scheme. Selected bond lengths (Å) and angles (°) are as follows: Fe(1)–P(1) 2.1694(6), Fe(1)–S(1) 2.2531(6), Fe(1)–S(2) 2.2699(6), Fe(1)–Fe(2) 2.4973(4), Fe(2)–S(1) 2.2679(6), Fe(2)–S(2) 2.2705(6), Fe(3)–S(3) 2.2524(7), Fe(3)–S(4) 2.2577(6), Fe(3)–Fe(4) 2.5156(5), Fe(4)–S(3) 2.2481(7), Fe(4)–S(4) 2.2539(7), Fe(5)–S(6) 2.2472(6), Fe(5)–S(5) 2.2559(6), Fe(5)–Fe(6) 2.5108(4), Fe(6)–S(5) 2.2462(6), Fe(6)–S(6) 2.2579(6), P(1)–O(1) 1.5941(15), P(1)–O(3) 1.6040(15), P(1)–O(1) 1.6054(15), C(12)–Fe(1)–C(11) 90.60(10), C(12)–Fe(1)–P(1) 105.97(7), C(11)–Fe(1)–P(1) 95.12(7), C(11)–Fe(1)–S(1) 87.31(7), P(1)–Fe(1)–S(1) 100.08(2), C(12)–Fe(1)–S(2) 86.98(7), P(1)–Fe(1)–S(2) 108.40(2), S(1)–Fe(1)–S(2) 84.57(2), C(12)–Fe(1)–Fe(2) 98.28(7), C(11)–Fe(1)–Fe(2) 100.36(7), P(1)–Fe(1)–Fe(2) 151.00(2), S(1)–Fe(1)–Fe(2) 56.753(17), S(2)–Fe(1)–Fe(2) 56.643(16), Fe(1)–S(1)–Fe(2) 67.060(18), and Fe(1)–S(2)–Fe(2) 66.738(18)

phosphite phosphorus atom is coordinated to Fe(1) in the $[(\mu\text{-SR})_2\text{Fe}_2(\text{CO})_5]$ unit. All $[(\mu\text{-SR})_2\text{Fe}_2]$ centers adopt a butterfly geometry with N-substituted azadithiolate bridging ligands forming two fused six-membered metallocycles with the iron atoms. The metallocycles corresponding to Fe(1), Fe(3), and Fe(5) adopt boat conformations, with the chelated $[(\mu\text{-SR})_2\text{Fe}_2(\text{CO})_5]$ unit showing a Fe(1)⋯N(1) distance of 3.635 Å, considerably longer than the Fe(3)⋯N(2), and Fe(5)⋯N(3) distances of ca. 2.25 Å found in the terminally bonded [Fe–Fe] units. This longer Fe⋯N distance could be due to chelation restraints. The Fe–Fe bond lengths lie in the range found for similar μ -(phenylazanediy)bis-(methanethiolato) diiron structures (2.489–2.595 Å) (Figure 2).⁵³

The results above show that the ability of the P atom in complexes to coordinate to metal centers (intramolecularly) is excellent. For these complexes, the coordination of the P atom to the Fe center is allowed by the flexible structure of the ethanalamine tether (for **4a**) or the *o*-substituted aromatic tether in **4b**. The structure of complex **2** prevents this intramolecular coordination, leaving the P atom available for coordination to other metal centers.

Coordination of Phosphite Complex 2 to Pd(II) and Pt(II) Centers. First, the preparation of Pd and Pt complexes derived from phosphite **2** was studied. Upon treatment of complex **2** with *cis*-[PdCl₂(MeCN)₂] and *cis*-[PtCl₂(DMSO)₂] in CH₂Cl₂ at room temperature, the corresponding [M-bis(phosphite)Cl₂] square-planar complexes **5a** (M = Pd) and **5b** (M = Pt) were obtained in high yields (99% and 83%, respectively) (Scheme 3). Complexes **5a** and **5b** were isolated as red solids and were fully characterized by NMR and IR

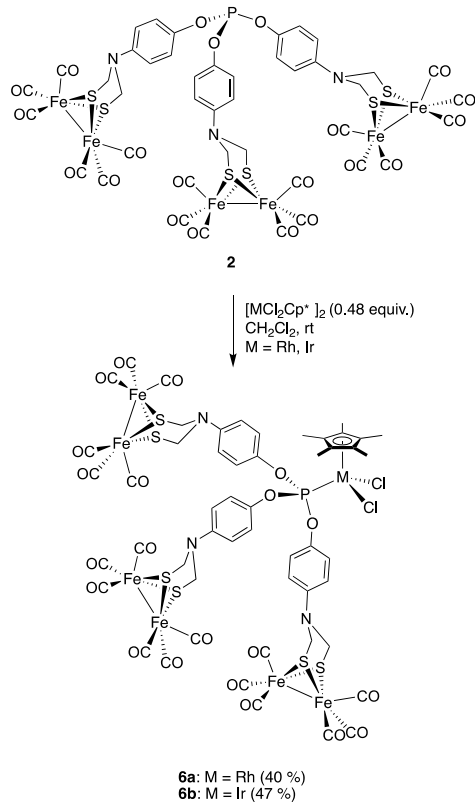
Scheme 3. Synthesis of Complexes **5a** (Pd) and **5b** (Pt)



spectroscopy, as well as elemental analysis. Resonances due to coordinated MeCN and DMSO were not observed in their ¹H NMR spectra, supporting the coordination of two phosphite groups to the Pd or Pt centers. For each compound, only one signal corresponding to the equivalent phosphite moieties was obtained in the ³¹P{¹H} NMR spectra: 85.15 ppm for **5a** and 61.31 ppm (*J*_{P–Pt} = 5736.8 Hz) for compound **5b**. Unfortunately, we were unable to obtain suitable single crystals of **5a** and **5b** to unambiguously characterize their spatial arrangement. The *cis*-geometry has been assigned by comparison to previously described complexes.^{54–56} The ³¹P{¹H} NMR shift and ³¹P–¹⁹⁵Pt constant coupling of **5b** compare to the spectroscopical data reported for other *cis*-[PtCl₂(P(OAr))₂] complexes. Additionally, only phosphites with large Tolman cone angles, bearing *ortho*- and *meta*-substituted aryl groups, have been described to afford the corresponding *trans*-isomers.^{56–58} It is noteworthy that **5a** and **5b** contain six [FeFe] units in their structures.

Coordination of Phosphite Complex 2 to Rh(III) and Ir(III) Centers. Once the coordination ability of complex **2** to the Pd and Pt centers was studied, the reactivity with Rh and Ir complexes was evaluated. Thus, complex **2** was reacted with the dinuclear [MCl₂Cp*]₂ species (M = Rh, Ir) in CH₂Cl₂ at room temperature (Scheme 4). Compounds **6a** and **6b**, where one phosphite unit is coordinated to the metal center, were obtained in 40% and 47% yields, respectively, after purification by column chromatography over neutral Al₂O₃. These compounds were fully characterized by NMR and IR spectroscopy and elemental analysis. In the ³¹P{¹H} NMR spectrum, a phosphorus signal attributable to a phosphite group was observed as a doublet (*J*_{P–Rh} = 240.2 Hz) at 107.08

Scheme 4. Synthesis of Complexes 6a (Rh) and 6b (Ir)



ppm for the Rh complex (6a) and as a singlet at 65.23 ppm for the Ir derivative (6b).

Electrochemistry. Phosphite 2 bearing an uncoordinated phosphorus atom experiences a first quasi-reversible reduction at -1.79 V and a second one at -1.99 V. This is the usual behavior of $[(\mu\text{-ADT}^R)\text{Fe}_2(\text{CO})_6]$ complexes and has been attributed to the $[\text{Fe}^{\text{I}}\text{Fe}^{\text{I}}]/[\text{Fe}^{\text{I}}\text{Fe}^0]$ and $[\text{Fe}^{\text{I}}\text{Fe}^{\text{I}}]/[\text{Fe}^{\text{I}}\text{Fe}^0]$ processes, respectively.^{59–69}

Compounds 4a and 4b have two differently substituted [FeFe] clusters. Both complexes experience two reduction events: the first wave appears at -1.82 V for 4a (irreversible) and -1.79 V (quasi-reversible) for 4b, and the second at -2.11 and -2.06 V (both quasi-reversible) for 4a and 4b, respectively. According to the literature, the substitution of one CO ligand by a PPh₃ ligand in $[(\mu\text{-ADT}^R)\text{Fe}_2(\text{CO})_6]$ complexes provokes a notable cathodic displacement.^{50,70} Therefore, the first reduction wave for these complexes is attributable to the reduction of the $[(\mu\text{-SR})_2\text{Fe}_2(\text{CO})_5]$ units, while the second wave is, in principle, attributable to the reduction of the second $[(\mu\text{-SR})_2\text{Fe}_2(\text{CO})_5(\text{P}(\text{OR})_3)]$ cluster (see Table 1 and Figure 3). Additionally, compounds 2, 4a, and 4b experience an irreversible oxidation event above 0.5 V, which is most likely due to the $[\text{Fe}^{\text{I}}\text{Fe}^{\text{I}}]/[\text{Fe}^{\text{I}}\text{Fe}^{\text{II}}]$ oxidation.

To support these asseverations, DFT calculations (M06 level, see the Experimental Section) were carried out in the model complex 7. The LUMO of the neutral species and the SOMO of the radical anion 7^{•−} are represented in Figure 4. The LUMO is centered in the $[\text{Fe}_2(\text{CO})_6]$ moiety, thus corroborating the hypothesis mentioned above that this species is the one experiencing the first reduction. The SOMO of the anion radical 7^{•−} is located at the $[(\mu\text{-SR})_2\text{Fe}_2(\text{CO})_5(\text{P}(\text{OR})_3)]$ moiety and thus the second reduction should occur in this bimetallic center.

Table 1. Electrochemical Data of Complexes 2, 4a, 4b, 5a, 5b, 6a, and 6b^a

entry	complex	reduction		oxidation
		E_{pc}	E_{pa}	E_{pa}
1	2	-1.79	-1.58	0.58
		-1.99	-1.89	
2	4a	-1.82	-1.95	0.42
		-2.11		
3	4b	-1.79	-1.65	0.72
		-2.06		
4	5a	-1.36	-1.56	0.60
		-1.82		
5	5b	-1.83	-1.59	0.58
6	6a	-1.84	-1.62	0.59
7	6b	-1.75	-1.56	0.62

^aPotentials given in V vs Fc⁺/Fc. Data were obtained from Figures 3 and 5.

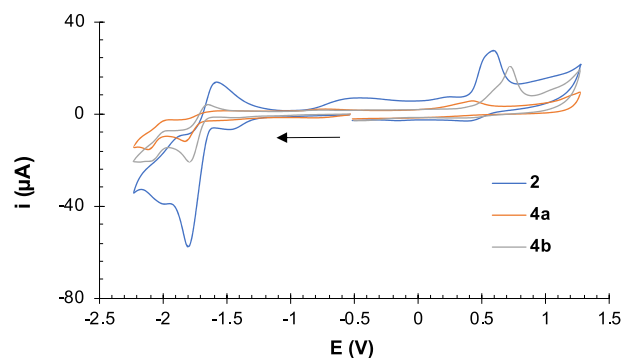


Figure 3. Cyclic voltammograms (CVs) of compounds 2, 4a, and 4b. Data were obtained from 10^{-3} M CH₂Cl₂ solutions containing 10^{-1} M [NBu₄]PF₆ as the supporting electrolyte at 25 °C. The counter electrode was Pt, the working electrode was glassy carbon, potentials are given in V vs Fc⁺/Fc, and the scan rate was 100 mV/s.

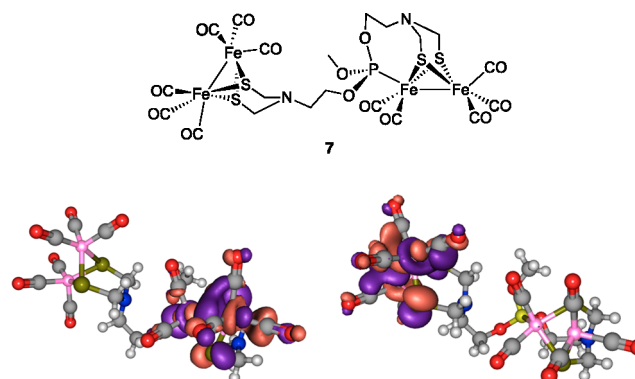


Figure 4. LUMO (right) of model 7 and SOMO (left) of radical anion 7^{•−}.

Complexation of compound 2 to form heterometallic complexes 5 and 6 results in the disappearance of the reduction waves at more negative potentials, while the remaining reduction wave appears at potentials similar to the free product 2 (Table 1 and Figure 5). The position of this wave is nearly independent of the metal complexed to the phosphorus atom and the complex geometry (square-planar 5 or half-sandwich 6). Additionally, complex 5a shows a

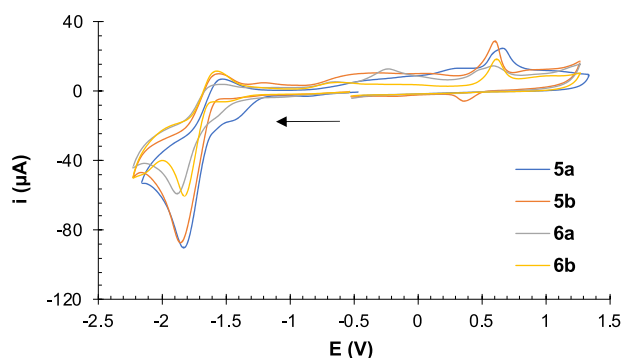


Figure 5. Cyclic voltammograms (CVs) of compounds **5a**, **5b**, **6a**, and **6b**. Data were obtained from 10^{-3} M CH_2Cl_2 solutions containing 10^{-1} M $[\text{NBu}_4]\text{PF}_6$ as the supporting electrolyte at 25°C . The counter electrode was Pt, the working electrode was glassy carbon, potentials are given in V vs Fc^+/Fc , and the scan rate was 100 mV/s.

reduction wave at -1.36 V that is associated with the reduction of the $\text{Pd}(\text{II})$ center.^{71,72}

DFT calculations carried out in the model complex **8** show that the LUMO of this molecule is centered in the fragment $[(\mu\text{-SR})_2\text{Fe}_2(\text{CO})_5]$ (Figure 6), which makes the observed reduction similar to the first reduction of model complex **7** and assignable to the $[\text{Fe}^{\text{I}}\text{Fe}^{\text{I}}]/[\text{Fe}^{\text{I}}\text{Fe}^0]$ process.

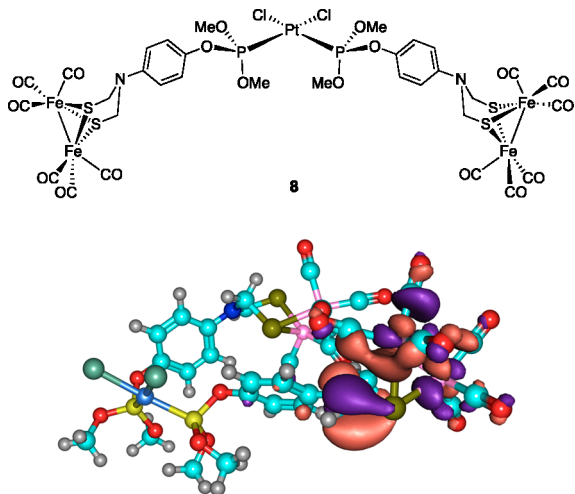


Figure 6. LUMO of model complex **8**.

The electrochemistry of compounds **2**, **4**, **5**, and **6** in the presence of increasing amounts of AcOH was studied next. Thus, the CVs of complexes **2**, **4a**, and **4b** in the presence of AcOH (Figure 7) demonstrate the absence of electrocatalytic activity at the first reduction level, while the current intensity of the second wave increases with the amount of acid. This is the expected behavior for complexes of the general formula $[(\mu\text{-ADT}^{\text{R}})\text{Fe}_2(\text{CO})_6]$.

Additionally, in all cases, a new wave appears at -1.40 V upon the addition of acid, and its intensity increases as the amount of acid does. This is especially notorious in complex **4b** (Figure 7). It can be thought that this process arises from the reduction of species formed by the protonation of the neutral complexes. To discard this possibility, a ^1H and ^{31}P NMR study of **4b** in the presence of increasing amounts of acid was performed. Complex protonation was not observed, even

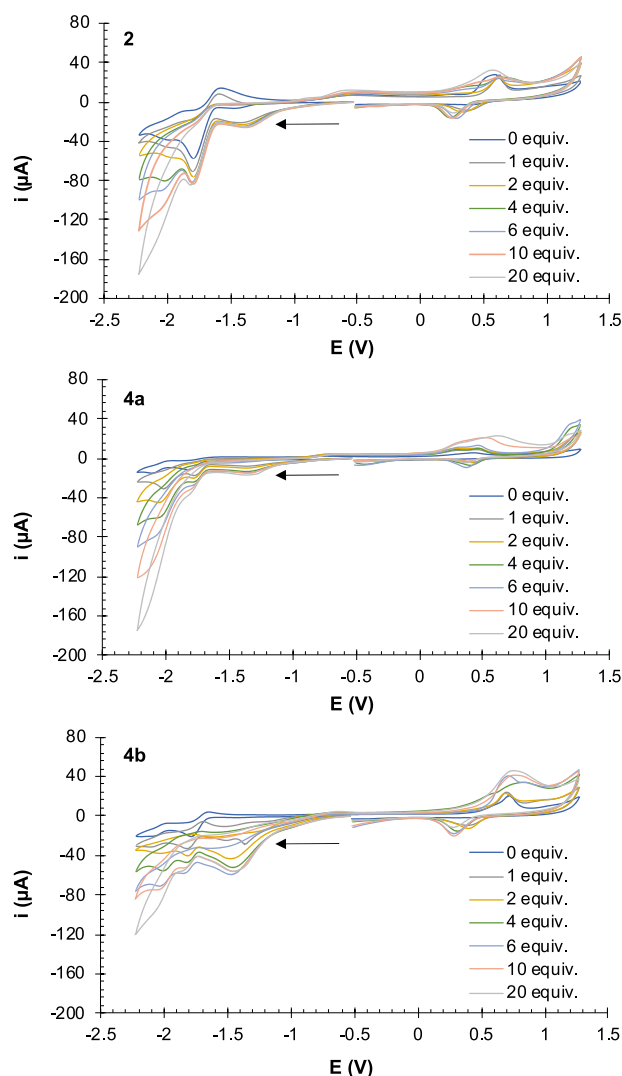


Figure 7. Cyclic voltammograms (CVs) of compounds **2**, **4a**, and **4b** in the presence of increasing amounts of AcOH . Data were obtained from 10^{-3} M CH_2Cl_2 solutions containing 10^{-1} M $[\text{NBu}_4]\text{PF}_6$ as the supporting electrolyte at 25°C . The counter electrode was Pt, the working electrode was glassy carbon, potentials are given in V vs Fc^+/Fc , and the scan rate was 100 mV/s.

after the addition of 20 equiv of acetic acid (Figures S16 and S17).⁷³ Therefore, the wave at -1.40 V should be due to a species resulting from the electrochemical decomposition of the compounds. In fact, when the CV of **4b** was recorded in the -0.55 to -2.24 V range, in the presence of increasing amounts of AcOH , this wave was not observed (Figure 8). For this reason, the following electrocatalytic studies were registered in the -0.55 to -2.24 V range.

In the CVs of complexes **5a** and **5b**, the waves around -1.80 V show a current increase with the successive additions of AcOH . Additionally, a new wave that grows with the amount of AcOH appears around -1.40 V for both complexes (Figure 9). Reduction of the $\text{Pt}(\text{II})$ nucleus should occur at more negative potentials according to the literature data.^{74,75} Alternatively, $\text{Pd}(\text{II})$ phosphite complexes experience two sequential reduction processes at -0.76 and -1.20 V.⁷⁶ Complexes **5** are stable in the presence of increasing amounts of acetic acid, as observed by ^1H NMR spectroscopy analysis (see Figures S24 and S25). Therefore, the wave around -1.40

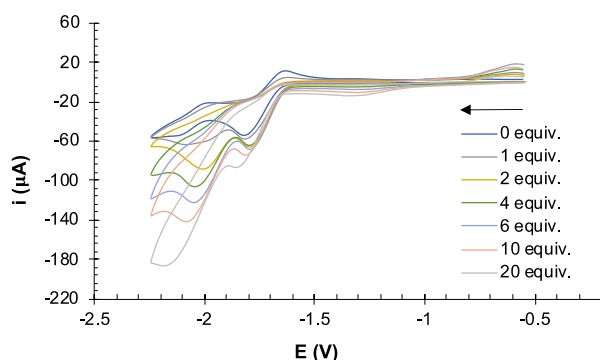


Figure 8. Cyclic voltammograms (CVs) of compound **4b** in the presence of increasing amounts of AcOH (0–20 equiv). Data were obtained from 10^{-3} M CH_2Cl_2 solutions containing 10^{-1} M $[\text{NBu}_4]\text{PF}_6$ as the supporting electrolyte at 25°C . The counter electrode was Pt, the working electrode was glassy carbon, potentials are given in V vs Fc^+/Fc , and the scan rate was 100 mV/s.

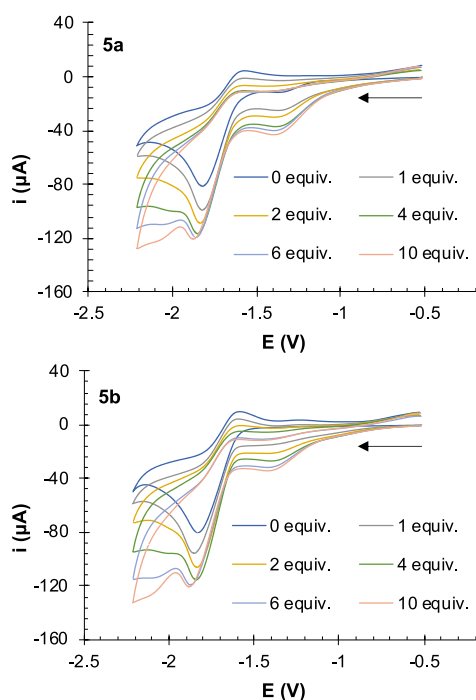


Figure 9. Cyclic voltammograms (CVs) of compounds **5a** and **5b** in the presence of increasing amounts of AcOH (0–10 equiv). Data were obtained from 10^{-3} M CH_2Cl_2 solutions containing 10^{-1} M $[\text{NBu}_4]\text{PF}_6$ as the supporting electrolyte at 25°C . The counter electrode was Pt, the working electrode was glassy carbon, potentials are given in V vs Fc^+/Fc , and the scan rate was 100 mV/s.

V should be caused by an acid-promoted by-reaction along the electrochemical process.

In contrast, the waves at -1.80 V in the half-sandwich complexes **6a** and **6b** experience an increase in the current intensity, but no new waves appear in the presence of acid (Figure 10).

CONCLUSIONS

Phosphite **2** having three $[(\mu\text{-SR})_2\text{Fe}_2(\text{CO})_6]$ ($\text{R} = 4\text{-hydroxyphenyl}$) units is easily accessible in good yields from $[(\mu\text{-SR})_2\text{Fe}_2(\text{CO})_6]$ ($\text{R} = 4\text{-HOC}_6\text{H}_4$) (**1a**) by a reaction with PCl_3 . The open-chain derivative $[(\mu\text{-SR})_2\text{Fe}_2(\text{CO})_6]$ ($\text{R} = \text{CH}_2\text{CH}_2\text{OH}$) (**1b**) and the isomeric complex $[(\mu\text{-}$

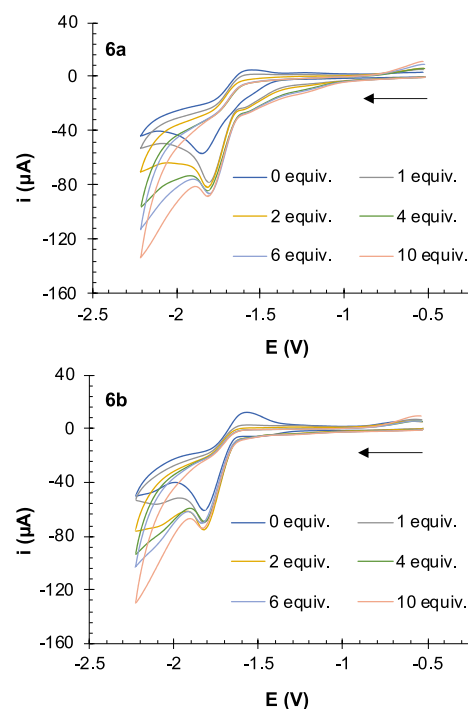


Figure 10. Cyclic voltammograms (CVs) of compounds **6a** and **6b** in the presence of increasing amounts of AcOH (0–10 equiv). Data were obtained from 10^{-3} M CH_2Cl_2 solutions containing 10^{-1} M $[\text{NBu}_4]\text{PF}_6$ as the supporting electrolyte at 25°C . The counter electrode was Pt, the working electrode was glassy carbon, potentials are given in V vs Fc^+/Fc , and the scan rate was 100 mV/s.

$\text{SR})_2\text{Fe}_2(\text{CO})_6]$ ($\text{R} = 2\text{-HOC}_6\text{H}_4$) (**1c**) also form the hexametallic complexes, which evolve in situ into the cyclic complexes **4a** and **4b**, respectively, by spontaneous intramolecular CO substitution in one of the $[\text{FeFe}]$ fragments. Coordination of complex **2** to $[\text{PdCl}_2(\text{MeCN})_2]$ or $[\text{PtCl}_2(\text{DMSO})_2]$ forms heterometallic square-planar complexes having 12 Fe centers in their structures. The coordination of phosphite **2** occurs in excellent yields. Analogously, the coordination of complex **2** to $[\text{MCl}_2\text{Cp}^*]_2$ ($\text{M} = \text{Rh}, \text{Ir}$) forms half-sandwich complexes **6a** and **6b** in 40% and 47% yields, respectively. Complexes **5** and **6** demonstrate the ability of complex **2** to form different heterometallic complexes under mild reaction conditions. This may be the first step to producing nanoparticles to anchor several $[\text{FeFe}]$ -hydrogenase mimics to surfaces in a straightforward manner.

The electrochemical behavior of complexes **2** and **4** in a DCM solution and upon the addition of AcOH is similar to that of ADT derivatives, showing electrocatalytic activity about -1.80 V. Nevertheless, complexes **2** and **4** experience electrochemical decomposition, as demonstrated when the CV was recorded only in the anodic region.

The successive additions of AcOH also cause an increase in current intensity in the wave at -1.80 V for heterometallic complexes **5** and **6**. However, the appearance of a new wave around -1.40 V in complexes **5** points to the acid-induced decomposition of the molecule by the decoordination of one Cl^- ligand in the square-planar $\text{Pt}(\text{II})$ complex.

In summary, the ability of phosphite **2** to act as a carrier of three units of $[(\mu\text{-ADT}^{\text{R}})\text{Fe}(\text{CO})_6]$ to the coordination spheres of different metal complexes has been demonstrated. The electrochemical and electrocatalytic properties of the heteropolymetallic complexes are affected by the complexation

of the new metal center, which may be of interest for the future preparation of nanoparticles and the anchorage of these units to surfaces.

EXPERIMENTAL SECTION

General Information. Unless stated otherwise, all the reactions were carried out under an Ar atmosphere using anhydrous solvents. The reaction workup was performed in air. Commercially available reagents were used as received without further purification. Compounds **1a**⁴⁹ and **1c**⁴⁶ were prepared following literature procedures. ¹H, ¹³C{¹H}, and ³¹P{¹H} NMR spectra were recorded at ambient temperature in CDCl₃ on a Bruker 300 or 500 MHz spectrometer. Chemical shifts are expressed in part per millions and are referenced to residual solvent peaks (¹H and ¹³C{¹H}) or to an external reference (85% H₃PO₄ aqueous solution for ³¹P{¹H}). FTIR spectra (ATR) were recorded as films (by slowly evaporating CHCl₃ solutions of the compounds) on a Bruker Alpha spectrometer. ESI-HRMS was performed on an Agilent 6500 accurate mass spectrometer with a Q-TOF analyzer. Elemental analyses were carried out on an elemental microanalyzer LECO CHNS-932. Cyclic voltammograms were recorded using a Metrohm Autolab Potentiostat model PGSTAT302N with a 3 mm glassy carbon working electrode, 3 M Ag/AgCl as the reference electrode, and a 2 mm Pt wire counter electrode. All the measurements were performed under Ar at 25 °C from CH₂Cl₂ solutions containing 10^{−1} M [NBu₄]⁺PF₆[−] as the supporting electrolyte, with analyte concentrations of 10^{−3} M.

Computational Details. All calculations were performed at the DFT level using the M06 functional^{77–79} with an ultrafine integration grid⁸⁰ in conjunction with the D3 dispersion correction suggested by Grimme,⁸¹ as implemented in Gaussian 16.⁸² P, S, Cl, Fe, and Pt atoms were described using the scalar-relativistic Stuttgart–Dresden SDD pseudopotential⁸³ and its associated double- ζ basis set complemented with a set of f-polarization functions.⁸⁴ The 6-31G** basis set was used for the H, C, N, and O atoms.^{85,86} All structures were fully optimized in MeCN ($\epsilon = 8.93$) using the SMD continuum model.⁸⁷ All energies are Gibbs energies in dichloromethane at 298 K.

Compound 1b. In a 100 mL round-bottom flask, [(μ -S₂)-Fe₂(CO)₆] (506 mg, 1 equiv) was dissolved in 22 mL of THF. The solution was cooled to −78 °C and then 1 M LiEt₃BH in THF (3.47 mL, 2 equiv) was added dropwise. After 30 min, TFA (0.27 mL, 2 equiv) was added dropwise, and the new mixture was stirred for 15 min. Then, to the mixture was slowly added 37% aqueous CH₂O (0.26 mL, 2 equiv). The reaction mixture was warmed to room temperature and stirred for 1 h. After this time, 2-aminophenol (189 mg, 1 equiv) was added as a solid, and the resulting mixture was stirred overnight. The solvent was removed under reduced pressure, and the residue was purified by column chromatography (SiO₂, 8:2 hexane/EtOAc). Compound **1b** was obtained as a red solid in a 62% yield (511 mg). ¹H NMR (300 MHz, CDCl₃) δ : 7.08 (t, $J = 7.3$ Hz, 1H_{Ar}), 6.98–6.77 (m, 3H_{Ar}), 5.90 (br, 1H_{OH}), 3.57 (s, 4H, CH₂) ppm. ¹³C{¹H} NMR (75 MHz, CDCl₃) δ : 207.7 (CO), 150.0 (C_{Ar}), 137.1 (C_{Ar}), 127.6 (CH_{Ar}), 122.4 (CH_{Ar}), 120.9 (CH_{Ar}), 116.3 (CH_{Ar}), 51.9 (CH₂) ppm. IR (film): ν_{OH} 3475 (br); $\nu_{C=O}$ 2074 (s), 2030 (vs), 1989 (vs) cm^{−1}. ESI-HRMS m/z : calcd. for C₁₄H₁₀Fe₂NO₂S₂ ([M + H]⁺) 479.8598, found ([M + H]⁺) 479.8612.

General Procedure for Preparation [FeFe]-Phosphite Derivatives (2 and 4). In a round-bottom flask, the corresponding [FeFe] complex **1** (3 equiv) was dissolved in CH₂Cl₂, and to the mixture was added anhydrous Et₃N (6 equiv). The solution was cooled to 0 °C, and to the mixture was added PCl₃ (1 equiv) dropwise. The reaction mixture was refluxed for 2 h. After this time, the solution was allowed to reach room temperature and the solvent was evaporated. The crude materials were purified as indicated in each case.

Complex 2. The general procedure was followed with 1.97 g of compound **1a**, 50 mL of CH₂Cl₂, 1.14 mL of anhydrous Et₃N, and 0.12 mL of PCl₃. Upon evaporation, the reaction crude was extracted with Et₂O until the organic layer was colorless. The combined organic

layers were evaporated under reduced pressure, and the resulting red solid was purified by column chromatography (activated neutral Al₂O₃, activity I, 7:3 hexane/EtOAc). The product was precipitated with Et₂O to afford compound **2** as a red solid in a 75% yield (1.50 g). ¹H NMR (500 MHz, CDCl₃) δ : 7.11 (d, $J = 9.0$ Hz, 6H_{Ar}), 6.72 (d, $J = 9.0$ Hz, 6H_{Ar}), 4.31 (s, 12H, CH₂) ppm. ¹³C{¹H} NMR (126 MHz, CDCl₃) δ : 207.1 (CO), 145.3 (d, $J_{C-P} = 3$ Hz, C_{Ar}), 141.6 (C_{Ar}), 122.3 (d, $J_{C-P} = 6$ Hz, CH_{Ar}), 117.3 (CH_{Ar}), 50.2 (CH₂) ppm. ³¹P{¹H} NMR (202 MHz, CDCl₃) δ : 128.59 ppm. IR (film): $\nu_{C=O}$ 2074 (s), 2034 (vs), 1995 (vs) cm^{−1}. Anal. Calcd (%) for C₄₂H₂₄Fe₆N₃O₂₁PS₆ + 0.25Et₂O: C, 34.81; H, 1.80; N, 2.83. Found: C, 34.74; H, 2.11; N, 2.87.

Complex 4a. Following the general procedure from 600 mg of compound **1b**, 18 mL of CH₂Cl₂, 0.39 mL of anhydrous Et₃N, and 0.04 mL of PCl₃, 380 mg (63% yield) of compound **4a** was obtained as a red solid upon column chromatography (SiO₂, 8:2 hexane/EtOAc). ¹H NMR (300 MHz, CDCl₃) δ : 4.04–3.86 (m, 8H), 3.78–3.66 (m, 10H), 3.10 (t, $J = 5.3$ Hz, 4H), 2.85 (t, $J = 4.2$ Hz, 2H) ppm. ¹³C{¹H} NMR (75 MHz, CDCl₃) δ : 211.5 (d, $J_{C-P} = 13.0$ Hz, CO), 209.0 (CO), 207.8 (CO), 63.4 (d, $J_{C-P} = 7.0$ Hz, CH₂), 62.0 (CH₂), 59.6 (CH₂), 57.2 (d, $J_{C-P} = 7.0$ Hz, CH₂), 53.6 (CH₂), 52.43 (CH₂) ppm. ³¹P{¹H} NMR (122 MHz, CDCl₃) δ : 186.78 ppm. IR (film): $\nu_{C=O}$ 2072 (s), 2027 (vs), 1961 (vs) cm^{−1}. ESI-HRMS m/z : calcd. for C₂₉H₂₄Fe₆N₃O₂₀PS₆ ([M + H]⁺) 1293.5190, found ([M + H]⁺) 1293.5158.

Complex 4b. Following the general procedure from 504 mg of compound **1c**, 14 mL of CH₂Cl₂, 0.29 mL of anhydrous Et₃N, and 0.03 mL of PCl₃, 418 mg (83% yield) of compound **4b** was obtained as a red solid upon column chromatography (SiO₂, 9:1 hexane/EtOAc). ¹H NMR (300 MHz, CDCl₃) δ : 7.55 (d, $J = 8.0$ Hz, 2H_{Ar}), 7.34–7.19 (m, 4H_{Ar}), 7.15 (t, $J = 7.6$ Hz, 3H_{Ar}), 6.95 (t, $J = 7.8$ Hz, 1H_{Ar}), 6.80 (d, $J = 8.0$ Hz, 1H_{Ar}), 6.38 (d, $J = 8.1$ Hz, 1H_{Ar}), 3.96 (m, 12H, CH₂) ppm. ¹³C{¹H} NMR (75 MHz, CDCl₃) δ : 209.7 (d, $J = 7.0$ Hz, CO), 207.8 (CO), 207.4 (CO), 146.7 (d, $J = 9.0$ Hz, C_{Ar}), 142.9 (d, $J = 8.0$ Hz, C_{Ar}), 141.7 (d, $J = 3.0$ Hz, C_{Ar}), 139.7 (d, $J = 4.0$ Hz, C_{Ar}), 127.2 (CH_{Ar}), 126.8 (CH_{Ar}), 126.5 (CH_{Ar}), 126.2 (CH_{Ar}), 124.4 (CH_{Ar}), 123.8 (CH_{Ar}), 123.6 (CH_{Ar}), 122.8 (d, $J = 5.0$ Hz, CH_{Ar}), 53.3 (CH₂), 53.3 (CH₂), 51.4 (CH₂). ³¹P{¹H} NMR (122 MHz, CDCl₃) δ : 175.91 ppm. IR (film): $\nu_{C=O}$ 2074 (s), 2056 (s), 2032 (vs), 1990 (vs) cm^{−1}. ESI-HRMS m/z : calcd. for C₄₁H₂₅Fe₆N₃O₂₀PS₆ ([M + H]⁺) 1437.5190, found ([M + H]⁺) 1437.5181.

Thiophosphate 3. Complex **1a** (285 mg, 3 equiv) was dissolved in 2.5 mL of CH₂Cl₂ in a 5 mL microwave vial, and to the mixture was added 0.2 mL (6 equiv) of anhydrous Et₃N. The solution was cooled to 0 °C, and to the mixture was added 20 μ L (1 equiv) of PSCl₃ dropwise. The reaction mixture was heated at 65 °C for 6 h in a microwave reactor. After this time, the solution was allowed to reach room temperature and the solvent was evaporated. Complex **3** was isolated as a red solid in a 43% yield (127 mg) upon column chromatography (SiO₂, 7:3 hexane/EtOAc). ¹H NMR (300 MHz, CDCl₃) δ : 7.20 (d, $J = 9.1$ Hz, 6H_{Ar}), 6.75 (d, $J = 9.1$ Hz, 6H_{Ar}), 4.32 (s, 12H, CH₂) ppm. ¹³C{¹H} NMR (75 MHz, CDCl₃) δ : 207.1 (CO), 144.4 (C_{Ar}), 142.7 (C_{Ar}), 122.7 (CH_{Ar}), 116.9 (CH_{Ar}), 50.1 (CH₂) ppm. ³¹P{¹H} NMR (122 MHz, CDCl₃) δ : 54.81 ppm. IR (film): $\nu_{C=O}$ 2074 (s), 2030 (vs), 1991 (vs) cm^{−1}. Anal. Calcd (%) for C₄₂H₂₄Fe₆N₃O₂₁PS₇: C, 33.70; H, 1.62; N, 2.81. Found: C, 33.39; H, 1.79; N, 2.83.

General Procedure for Preparation of Square-Planar Complexes 5. In a 10 mL round-bottom flask, compound **2** (2 equiv), the corresponding [MCl₂L₂] (1 equiv; M = Pd, Pt) and CH₂Cl₂ were added. The mixture was stirred at room temperature for 24 h and the solvent was removed under reduced pressure. The purification procedure is specified below.

Complex 5a. Following the general procedure from 150 mg of compound **2**, 13.3 mg of [PdCl₂(MeCN)₂], and 5 mL of CH₂Cl₂. Upon evaporation, the residue was washed with Et₂O (4 \times 5 mL) to afford pure complex **5a** (163 mg, 99% yield) as a red solid. ¹H NMR (500 MHz, CDCl₃) δ : 7.11 (br s, 12H_{Ar}), 6.68 (br s, 12H_{Ar}), 4.37 (br s, 24H, CH₂) ppm. ¹³C{¹H} NMR (126 MHz, CDCl₃) δ : 206.9

(CO), 144.1 (C_{Ar}), 142.5 (C_{Ar}), 122.5 (CH_{Ar}), 117.1 (CH_{Ar}), 50.4 (CH_2) ppm. $^{31}P\{^1H\}$ NMR (202 MHz, $CDCl_3$) δ : 85.15 ppm. IR (film): $\nu_{C\equiv O}$ 2074 (s), 2030 (vs), 1987 (vs) cm^{-1} . Anal. Calcd (%) for $C_{84}H_{48}Cl_2Fe_{12}N_6O_{42}P_2PdS_{12} + H_2O$: C, 32.28; H, 1.61; N, 2.69. Found: C, 32.18; H, 1.93; N, 2.69.

Complex 5b. The general procedure was following using 200 mg of compound **2**, 26.4 mg of $[PtCl_2(DMSO)_2]$, and 4 mL of CH_2Cl_2 . Upon evaporation, the residue was washed with Et_2O (4×5 mL), and the obtained solid was further purified by column chromatography (SiO_2 , 4:6 hexane/ $EtOAc$) to afford pure complex **5b** (165 mg, 83% yield) as a red solid. 1H NMR (500 MHz, $CDCl_3$) δ : 7.10 (br s, $12H_{Ar}$), 6.66 (br s, $12H_{Ar}$), 4.36 (br s, $24H$, CH_2) ppm. $^{13}C\{^1H\}$ NMR (126 MHz, $CDCl_3$) δ : 206.9 (CO), 144.2 (C_{Ar}), 142.3 (C_{Ar}), 122.4 (CH_{Ar}), 116.8 (CH_{Ar}), 49.9 (CH_2) ppm. $^{31}P\{^1H\}$ NMR (202 MHz, $CDCl_3$) δ : 61.31 ($J_{P-Pt} = 5736.8$ Hz) ppm. IR (film): $\nu_{C\equiv O}$ 2074 (s), 2032 (vs), 1986 (vs) cm^{-1} . Anal. Calcd (%) for $C_{84}H_{48}Cl_2Fe_{12}N_6O_{42}P_2PtS_{12} + H_2O$: C, 31.39; H, 1.57; N, 2.61; Found: C, 31.39; H, 1.95; N, 2.61.

General Procedure for Preparation of Half-Sandwich Complexes 6. To a 25 mL round-bottom flask were added compound **2** (1 equiv), $[MCl_2Cp^*]_2$ (0.48 equiv, $M = Rh, Ir$), and CH_2Cl_2 . The mixture was stirred at room temperature overnight. After this time, the solvent was evaporated under reduced pressure. The reaction crude was purified by column chromatography (activated neutral Al_2O_3 activity I, 1:1 $CH_2Cl_2/EtOAc$).

Complex 6a. Following the general procedure from 209.5 mg of compound **2**, 42.2 mg of $[RhCl_2Cp^*]_2$, and 7 mL of CH_2Cl_2 , complex **6a** (95 mg, 40% yield) was obtained as a red solid. 1H NMR (500 MHz, $CDCl_3$) δ : 7.29 (br s, 6H, CH_{Ar}), 6.68 (br s, 6H, CH_{Ar}), 4.29 (br s, 12H, CH_2), 1.64 (br s, 15H, CH_3) ppm. $^{13}C\{^1H\}$ NMR (126 MHz, $CDCl_3$) δ : 207.1 (CO), 145.3 (d, $J_{C-P} = 12$ Hz, C_{ArO}), 142.2 (C_{Ar}), 122.5 (d, $J_{C-P} = 4$ Hz, CH_{Ar}), 116.8 (CH_{Ar}), 101.5 (br s, C_{Cp^*}), 50.3 (CH_2), 9.4 (CH_3) ppm. $^{31}P\{^1H\}$ NMR (202 MHz, $CDCl_3$) δ : 107.08 (d, $J_{P-Rh} = 240.2$ Hz) ppm. IR (film): $\nu_{C\equiv O}$ 2073 (s), 2029 (vs), 1981 (vs) cm^{-1} . Anal. Calcd (%) for $C_{52}H_{39}Cl_2Fe_6N_3O_{21}PRhS_6 + 0.5AcOEt$: C, 35.67; H, 2.38; N, 2.31. Found: C, 35.45; H, 2.66; N, 2.34.

Complex 6b. Following the general procedure from 209.5 mg of compound **2**, 54.3 mg of $[IrCl_2Cp^*]_2$, and 7 mL of CH_2Cl_2 , complex **6b** (120 mg, 47% yield) was obtained as a red solid. 1H NMR (500 MHz, $CDCl_3$) δ : 7.27 (d, $J = 8.4$ Hz, 6H, CH_{Ar}), 6.68 (d, $J = 8.4$ Hz, 6H, CH_{Ar}), 4.28 (s, 12H, CH_2), 1.57 (s, 15H, CH_3) ppm. $^{13}C\{^1H\}$ NMR (126 MHz, $CDCl_3$) δ : 207.1 (CO), 145.3 (d, $J_{C-P} = 11$ Hz, C_{ArO}), 142.2 (C_{Ar}), 122.5 (d, $J_{C-P} = 4$ Hz, CH_{Ar}), 116.8 (CH_{Ar}), 95.7 (C_{Cp^*}), 50.3 (CH_2), 8.9 (CH_3) ppm. $^{31}P\{^1H\}$ NMR (202 MHz, $CDCl_3$) δ : 65.23 ppm. IR (film): $\nu_{C\equiv O}$ 2073 (s), 2031 (vs), 1990 (vs) cm^{-1} . Anal. Calcd (%) for $C_{52}H_{39}Cl_2Fe_6IrN_3O_{21}PS_6$: C, 33.52; H, 2.11; N, 2.26; Found: C, 33.61; H, 2.36; N, 2.29.

■ ASSOCIATED CONTENT

SI Supporting Information

The Supporting Information is available free of charge at <https://pubs.acs.org/doi/10.1021/acs.organomet.2c00549>.

Synthesis and characterization of compounds **7** and **8**, electrochemical information, DFT coordinates, and NMR and IR spectra of all compounds (PDF)

xyz data for compounds **7** and **8** (TXT)

Accession Codes

CCDC 2209558 contains the supplementary crystallographic data for this paper. These data can be obtained free of charge via www.ccdc.cam.ac.uk/data_request/cif, or by emailing data_request@ccdc.cam.ac.uk, or by contacting The Cambridge Crystallographic Data Centre, 12 Union Road, Cambridge CB2 1EZ, UK; fax: +44 1223 336033.

■ AUTHOR INFORMATION

Corresponding Author

Miguel A. Sierra – Departamento de Química Orgánica, Facultad de Química, Universidad Complutense, 28040 Madrid, Spain; Center for Innovation in Advanced Chemistry (ORFEO–CINQA), Universidad Autónoma de Madrid, 28049 Madrid, Spain; orcid.org/0000-0002-3360-7795; Email: sierraor@ucm.es

Authors

Alejandro Torres – Departamento de Química Orgánica, Facultad de Química, Universidad Complutense, 28040 Madrid, Spain; Center for Innovation in Advanced Chemistry (ORFEO–CINQA), Universidad Autónoma de Madrid, 28049 Madrid, Spain; orcid.org/0000-0001-6767-7137

Diego J. Vicent – Departamento de Química Orgánica, Facultad de Química, Universidad Complutense, 28040 Madrid, Spain; Center for Innovation in Advanced Chemistry (ORFEO–CINQA), Universidad Autónoma de Madrid, 28049 Madrid, Spain

Alba Collado – Center for Innovation in Advanced Chemistry (ORFEO–CINQA) and Departamento de Química Inorgánica, Facultad de Ciencias, Universidad Autónoma de Madrid, 28049 Madrid, Spain; Institute for Advanced Research in Chemical Sciences (IAdChem), Universidad Autónoma de Madrid, 28049 Madrid, Spain; orcid.org/0000-0001-6215-1822

Mar Gómez-Gallego – Departamento de Química Orgánica, Facultad de Química, Universidad Complutense, 28040 Madrid, Spain; Center for Innovation in Advanced Chemistry (ORFEO–CINQA), Universidad Autónoma de Madrid, 28049 Madrid, Spain; orcid.org/0000-0002-8961-7685

Carmen Ramírez de Arellano – Center for Innovation in Advanced Chemistry (ORFEO–CINQA), Universidad Autónoma de Madrid, 28049 Madrid, Spain; Departamento de Química Orgánica, Universidad de Valencia, 46100 Valencia, Spain; orcid.org/0000-0002-8976-0318

Complete contact information is available at:

<https://pubs.acs.org/doi/10.1021/acs.organomet.2c00549>

Notes

The authors declare no competing financial interest.

■ ACKNOWLEDGMENTS

Support for this work under Grants PID2019-108429RB-I00 and RED2018-102387-T from the MCINN (Spain) is gratefully acknowledged. M.A.S. thanks the Fundación Ramón Areces for a grant from the XVIII Concurso Nacional de Ayudas a la Investigación en Ciencias de la Vida y de la Materia (CIVP18A3938). A.C. thanks the MINECO (Spain) for a Juan de la Cierva-Incorporación Fellowship.

■ REFERENCES

- (1) Lubitz, W.; Ogata, H.; Rüdiger, O.; Reijerse, E. Hydrogenases. *Chem. Rev.* **2014**, *114*, 4081–4148.
- (2) del Barrio, M.; Sensi, M.; Orain, C.; Baffert, C.; Dementin, S.; Fourmond, V.; Léger, C. Electrochemical Investigations of Hydrogenases and Other Enzymes That Produce and Use Solar Fuels. *Acc. Chem. Res.* **2018**, *51*, 769–777.
- (3) Fontecilla-Camps, J. C.; Volbeda, A.; Cavazza, C.; Nicolet, Y. Structure/Function Relationships of $[NiFe]$ - and $[FeFe]$ -Hydrogenases. *Chem. Rev.* **2007**, *107*, 4273–4303.

- (4) Greene, B. L. Progress and Opportunities in Photochemical Enzymology of Oxidoreductases. *ACS Catal.* **2021**, *11*, 14635–14650.
- (5) Morra, S. Fantastic [FeFe]-Hydrogenases and Where to Find Them. *Front. Microbiol.* **2022**, *13*, 853626.
- (6) Stripp, S. T.; Duffus, B. R.; Fourmond, V.; Léger, C.; Leimkühler, S.; Hirota, S.; Hu, Y.; Jasiewicz, A.; Ogata, H.; Ribbe, M. W. Second and Outer Coordination Sphere Effects in Nitrogenase, Hydrogenase, Formate Dehydrogenase, and CO Dehydrogenase. *Chem. Rev.* **2022**, *122*, 11900–11973.
- (7) Vignais, P. M.; Billoud, B. Occurrence, Classification, and Biological Function of Hydrogenases: An Overview. *Chem. Rev.* **2007**, *107*, 4206–4272.
- (8) Birrell, J. A.; Rodríguez-Maciá, P.; Reijerse, E. J.; Martini, M. A.; Lubitz, W. The catalytic cycle of [FeFe] hydrogenase: A tale of two sites. *Coord. Chem. Rev.* **2021**, *449*, 214191.
- (9) Li, Y.; Rauchfuss, T. B. Synthesis of Diiron(I) Dithiolato Carbonyl Complexes. *Chem. Rev.* **2016**, *116*, 7043–7077.
- (10) Wang, F.; Wang, W.-G.; Wang, H.-Y.; Si, G.; Tung, C.-H.; Wu, L.-Z. Artificial Photosynthetic Systems Based on [FeFe]-Hydrogenase Mimics: the Road to High Efficiency for Light-Driven Hydrogen Evolution. *ACS Catal.* **2012**, *2*, 407–416.
- (11) Schilter, D.; Camara, J. M.; Huynh, M. T.; Hammes-Schiffer, S.; Rauchfuss, T. B. Hydrogenase Enzymes and Their Synthetic Models: The Role of Metal Hydrides. *Chem. Rev.* **2016**, *116*, 8693–8749.
- (12) Prasad, P.; Selvan, D.; Chakraborty, S. Biosynthetic Approaches towards the Design of Artificial Hydrogen-Evolution Catalysts. *Chem. - Eur. J.* **2020**, *26*, 12494–12509.
- (13) Amaro-Gahete, J.; Pavliuk, M. V.; Tian, H.; Esquivel, D.; Romero-Salguero, F. J.; Ott, S. Catalytic systems mimicking the [FeFe]-hydrogenase active site for visible-light-driven hydrogen production. *Coord. Chem. Rev.* **2021**, *448*, 214172.
- (14) Gómez-Gallego, M.; Sierra, M. A. Deuteration mechanistic studies of hydrogenase mimics. *Inorg. Chem. Front.* **2021**, *8*, 3934–3950.
- (15) Kleinhaus, J. T.; Wittkamp, F.; Yadav, S.; Siegmund, D.; Apfel, U.-P. [FeFe]-Hydrogenases: maturation and reactivity of enzymatic systems and overview of biomimetic models. *Chem. Soc. Rev.* **2021**, *50*, 1668–1784.
- (16) Ekström, J.; Abrahamsson, M.; Olson, C.; Bergquist, J.; Kaynak, F. B.; Eriksson, L.; Sun, L.; Becker, H.-C.; Åkermark, B.; Hammarström, L.; Ott, S. Bio-inspired, side-on attachment of a ruthenium photosensitizer to an iron hydrogenase active site model. *Dalton Trans.* **2006**, 4599–4606.
- (17) Ott, S.; Borgström, M.; Kritikos, M.; Lomoth, R.; Bergquist, J.; Åkermark, B.; Hammarström, L.; Sun, L. Model of the Iron Hydrogenase Active Site Covalently Linked to a Ruthenium Photosensitizer: Synthesis and Photophysical Properties. *Inorg. Chem.* **2004**, *43*, 4683–4692.
- (18) Ott, S.; Kritikos, M.; Åkermark, B.; Sun, L. Synthesis and Structure of a Biomimetic Model of the Iron Hydrogenase Active Site Covalently Linked to a Ruthenium Photosensitizer. *Angew. Chem., Int. Ed.* **2003**, *42*, 3285–3288.
- (19) Sun, L.; Åkermark, B.; Ott, S. Iron hydrogenase active site mimics in supramolecular systems aiming for light-driven hydrogen production. *Coord. Chem. Rev.* **2005**, *249*, 1653–1663.
- (20) Na, Y.; Pan, J.; Wang, M.; Sun, L. Intermolecular Electron Transfer from Photogenerated Ru(bpy)³⁺ to [2Fe2S] Model Complexes of the Iron-Only Hydrogenase Active Site. *Inorg. Chem.* **2007**, *46*, 3813–3815.
- (21) Na, Y.; Wang, M.; Pan, J.; Zhang, P.; Åkermark, B.; Sun, L. Visible Light-Driven Electron Transfer and Hydrogen Generation Catalyzed by Bioinspired [2Fe2S] Complexes. *Inorg. Chem.* **2008**, *47*, 2805–2810.
- (22) Frederix, P. W. J. M.; Kania, R.; Wright, J. A.; Lamprou, D. A.; Ulijn, R. V.; Pickett, C. J.; Hunt, N. T. Encapsulating [FeFe]-hydrogenase model compounds in peptide hydrogels dramatically modifies stability and photochemistry. *Dalton Trans.* **2012**, *41*, 13112–13119.
- (23) Jones, A. K.; Lichtenstein, B. R.; Dutta, A.; Gordon, G.; Dutton, P. L. Synthetic Hydrogenases: Incorporation of an Iron Carbonyl Thiolate into a Designed Peptide. *J. Am. Chem. Soc.* **2007**, *129*, 14844–14845.
- (24) Apfel, U.-P.; Kowol, C. R.; Halpin, Y.; Kloss, F.; Kübel, J.; Görls, H.; Vos, J. G.; Keppler, B. K.; Morera, E.; Lucente, G.; Weigand, W. Investigation of amino acid containing [FeFe] hydrogenase models concerning pendant base effects. *J. Inorg. Biochem.* **2009**, *103*, 1236–1244.
- (25) Apfel, U.-P.; Kowol, C. R.; Morera, E.; Görls, H.; Lucente, G.; Keppler, B. K.; Weigand, W. Synthetic and Electrochemical Studies of [2Fe2S] Complexes Containing a 4-Amino-1,2-dithiolane-4-carboxylic Acid Moiety. *Eur. J. Inorg. Chem.* **2010**, *2010*, 5079–5086.
- (26) de Hatten, X.; Bothe, E.; Merz, K.; Huc, I.; Metzler-Nolte, N. A Ferrocene-Peptide Conjugate as a Hydrogenase Model System. *Eur. J. Inorg. Chem.* **2008**, *2008*, 4530–4537.
- (27) de Hatten, X.; Cournia, Z.; Huc, I.; Smith, J. C.; Metzler-Nolte, N. Force-Field Development and Molecular Dynamics Simulations of Ferrocene-Peptide Conjugates as a Scaffold for Hydrogenase Mimics. *Chem. - Eur. J.* **2007**, *13*, 8139–8152.
- (28) Cheng, M.; Wang, M.; Zhang, S.; Liu, F.; Yang, Y.; Wan, B.; Sun, L. Photocatalytic H₂ production using a hybrid assembly of an [FeFe]-hydrogenase model and CdSe quantum dot linked through a thiolato-functionalized cyclodextrin. *Faraday Discuss.* **2017**, *198*, 197–209.
- (29) Liang, W.-J.; Wang, F.; Wen, M.; Jian, J.-X.; Wang, X.-Z.; Chen, B.; Tung, C.-H.; Wu, L.-Z. Branched Polyethylenimine Improves Hydrogen Photoproduction from a CdSe Quantum Dot/[FeFe]-Hydrogenase Mimic System in Neutral Aqueous Solutions. *Chem. - Eur. J.* **2015**, *21*, 3187–3192.
- (30) Wang, F.; Liang, W.-J.; Jian, J.-X.; Li, C.-B.; Chen, B.; Tung, C.-H.; Wu, L.-Z. Exceptional Poly(acrylic acid)-Based Artificial [FeFe]-Hydrogenases for Photocatalytic H₂ Production in Water. *Angew. Chem., Int. Ed.* **2013**, *52*, 8134–8138.
- (31) Cohen, S. M.; Zhang, Z.; Boissonnault, J. A. Toward “metalloMOFzymes”: Metal-Organic Frameworks with Single-Site Metal Catalysts for Small-Molecule Transformations. *Inorg. Chem.* **2016**, *55*, 7281–7290.
- (32) Nath, I.; Chakraborty, J.; Verpoort, F. Metal organic frameworks mimicking natural enzymes: a structural and functional analogy. *Chem. Soc. Rev.* **2016**, *45*, 4127–4170.
- (33) Wang, W.; Yu, T.; Zeng, Y.; Chen, J.; Li, Y. An [Fe-Fe]-Hydrogenase Mimic Immobilized on MCM-41 for the Photochemical Production of Hydrogen in Pure Water. *Chin. J. Chem.* **2014**, *32*, 479–484.
- (34) Wang, W.; Yu, T.; Zeng, Y.; Chen, J.; Yang, G.; Li, Y. Enhanced photocatalytic hydrogen production from an MCM-41-immobilized photosensitizer-[Fe-Fe] hydrogenase mimic dyad. *Photochem. Photobiol. Sci.* **2014**, *13*, 1590–1597.
- (35) Williams, N. B.; Nash, A.; Yamamoto, N.; Patrick, M.; Tran, I. C.; Gu, J. Unraveling Activity and Decomposition Pathways of [FeFe] Hydrogenase Mimics Covalently Bonded to Silicon Photoelectrodes. *Adv. Mater. Interfaces* **2021**, *8*, 2001961.
- (36) Abaalkhail, S. J.; Abul-Futouh, H.; Görls, H.; Weigand, W. Electrochemical Behavior of Mono-Substituted [FeFe]-Hydrogenase H-Cluster Mimic Mediated by Stannylated Dithiolato Ligand. *Z. Anorg. Allg. Chem.* **2022**, *648*, No. e202200221.
- (37) Abul-Futouh, H.; Görls, H.; Weigand, W. Synthesis and Electrochemical Investigation of Mono- and Di-phosphite substituted [FeFe]-Hydrogenase H-Cluster Mimics. *Z. Anorg. Allg. Chem.* **2017**, *643*, 1615–1620.
- (38) Chen, F.-Y.; Wang, L.-H.; Tian, W.-J.; Liu, X.-F.; Li, Y.-L.; Liu, X.-H.; Jiang, Z.-Q. Synthesis, X-ray crystal structures, and electrochemistry of two diiron ethane-1,2-dithiolate complexes containing tris(4-trifluoromethylphenyl)phosphine or triethyl phosphite. *Inorg. Nano-Met. Chem.* **2021**, *52*, 512–518.
- (39) Daraosheh, A. Q.; Harb, M. K.; Windhager, J.; Görls, H.; Elkhateeb, M.; Weigand, W. Substitution Reactions at [FeFe]

Hydrogenase Models Containing [2Fe3S] Assembly by Phosphine or Phosphite Ligands. *Organometallics* **2009**, *28*, 6275–6280.

(40) Durgaprasad, G.; Das, S. K. 1,2-Ene dithiolate bridged diiron carbonyl-phosphine and -phosphite complexes in relevance to the active site of [FeFe]-hydrogenases: Synthesis, characterization and electrocatalysis. *J. Organomet. Chem.* **2012**, *717*, 29–40.

(41) Harb, M. K.; Windhager, J.; Daraosheh, A.; Görls, H.; Lockett, L. T.; Okumura, N.; Evans, D. H.; Glass, R. S.; Lichtenberger, D. L.; El-khateeb, M.; Weigand, W. Phosphane- and Phosphite-Substituted Diiron Diselenolato Complexes as Models for [FeFe]-Hydrogenases. *Eur. J. Inorg. Chem.* **2009**, *2009*, 3414–3420.

(42) Makouf, N. B.; Mousser, H. B.; Darchen, A.; Mousser, A. Carbon monoxide substitutions by trimethyl phosphite in diiron dithiolate complex: Fe-Fe bond cleavage, selectivity of the substitutions, crystal structures and electrochemical studies. *J. Organomet. Chem.* **2018**, *866*, 35–42.

(43) Song, L.-C.; Li, C.-G.; Gao, J.; Yin, B.-S.; Luo, X.; Zhang, X.-G.; Bao, H.-L.; Hu, Q.-M. Synthesis, Structure, and Electrocatalysis of Diiron C-Functionalized Propanedithiolate (PDT) Complexes Related to the Active Site of [FeFe]-Hydrogenases. *Inorg. Chem.* **2008**, *47*, 4545–4553.

(44) Yan, L.; Fang, Y.; Hu, K.; Liu, X.-F.; Li, Y.-L.; Liu, X.-H.; Jiang, Z.-Q. Diiron toluene-3,4-dithiolate complexes with a phosphine ligand ethyldiphenylphosphine or a phosphite ligand methyldiphenylphosphinite: synthesis, characterization, X-ray crystal structures, and electrochemistry. *Mol. Cryst. Liq. Cryst.* **2022**, *732*, 76–86.

(45) Phosphines have been profusely used as ligands to modulate the electronic properties and to study the mechanisms of HER by [FeFe]-hydrogenase mimics and to join two [FeFe] moieties. However, similar to phosphites, phosphines having [FeFe] moieties have not been used to incorporate these mimics to other metal complexes. For selected examples, see: (a) Zhang, F.; Woods, T. J.; Zhu, L.; Rauchfuss, T. B. Inhibition of [FeFe]-hydrogenase by formaldehyde: proposed mechanism and reactivity of FeFe alkyl complexes. *Chem. Sci.* **2021**, *12*, 15673–15681. (b) Greco, C. H₂ Binding and Splitting on a New-Generation [FeFe]-Hydrogenase Model Featuring a Redox-Active Decamethylferrocenyl Phosphine Ligand: A Theoretical Investigation. *Inorg. Chem.* **2013**, *52*, 1901–1908. (c) Meyer, R. L.; Zhandosova, A. D.; Biser, T. M.; Heilweil, E. J.; Stromberg, C. J. Photochemical dynamics of a trimethylphosphine derivatized [FeFe]-hydrogenase model compound. *Chem. Phys.* **2018**, *512*, 135–145. (d) Yan, L.; He, J.; Liu, X. F.; Li, Y. L.; Jiang, Z.-Q.; Wu, H.-K. Phosphine-substituted diiron 1,2-dithiolate complexes as the models for the active site of [FeFe]-hydrogenases. *J. Coord. Chem.* **2019**, *72*, 2531–2543. (e) Thomas, C. M.; Rudiger, O.; Liu, T.; Carson, C. E.; Hall, M. B.; Darensbourg, M. Y. Synthesis of carboxylic acid-modified [FeFe]-hydrogenase model complexes amenable to surface immobilization. *Organometallics* **2007**, *26*, 3976–3984. (f) Chatelain, L.; Breton, J. B.; Arrigoni, F.; Schollhammer, P.; Zampella, G. Geometrical influence on the non-biomimetic heterolytic splitting of H₂ by bio-inspired [FeFe]-hydrogenase complexes: a rare example of inverted frustrated Lewis pair based reactivity. *Chem. Sci.* **2022**, *13*, 4863–4873. (g) Zhao, P.-H.; Hu, M. Y.; Li, J. R.; Ma, Z.-Y.; Wang, Y.-Z.; He, J.; Li, Y.-L.; Liu, X. F. Influence of Dithiolate Bridges on the Structures and Electrocatalytic Performance of Small Bite-Angle PNP-Chelated Diiron Complexes Fe₂(μ-xdt)(CO)₄{κ²-(Ph₂P)₂NR} Related to [FeFe]-Hydrogenases. *Organometallics* **2019**, *38*, 385–394. (h) El-khateeb, M.; Abul-Futouh, H.; Alshurafa, H.; Görls, H.; Weigand, W. Influence of bidentate phosphine ligands on the chemistry of [FeFe]-hydrogenase model: Insight into molecular structures and electrochemical characteristics. *Appl. Organomet. Chem.* **2020**, *34*, No. e5940. (i) Song, L.-C.; Wang, L.-X.; Jia, G.-J.; Li, Q.-L.; Ming, J.-B. Synthesis, Structural Characterization, and Properties of Some Functionalized Phosphine-Containing Diiron Complexes As Models for the Active Site of [FeFe]-Hydrogenases. *Organometallics* **2012**, *31*, 5081–5088. (j) Gao, W.; Sun, J. L.; Åkermark, T.; Li, M. R.; Eriksson, L.; Sun, L. C.; Åkermark, B. Attachment of a Hydrogen-Bonding Carboxylate

Side Chain to an [FeFe]-Hydrogenase Model Complex: Influence on the Catalytic Mechanism. *Chem. - Eur. J.* **2010**, *16*, 2537–2546.

(46) Song, L.-C.; Luo, F.-X.; Tan, H.; Sun, X.-J.; Xie, Z.-J.; Song, H.-B. Synthesis, Structures, and Properties of Diiron Azadithiolate Complexes Containing a Subphthalocyanine Moiety as Biomimetic Models for [FeFe]-Hydrogenases. *Eur. J. Inorg. Chem.* **2013**, *2013*, 2549–2557.

(47) Zhang, Y.; Cai, Z.; Chi, Y.; Zeng, X.; Chen, S.; Liu, Y.; Tang, G.; Zhao, Y. Diphenyl Diselenide-Catalyzed Synthesis of Triaryl Phosphites and Triaryl Phosphates from White Phosphorus. *Org. Lett.* **2021**, *23*, 5158–5163.

(48) Gao, W.; Ekström, J.; Liu, J.; Chen, C.; Eriksson, L.; Weng, L.; Åkermark, B.; Sun, L. Binuclear Iron-Sulfur Complexes with Bidentate Phosphine Ligands as Active Site Models of Fe-Hydrogenase and Their Catalytic Proton Reduction. *Inorg. Chem.* **2007**, *46*, 1981–1991.

(49) Song, L.-C.; Yin, B.-S.; Li, Y.-L.; Zhao, L.-Q.; Ge, J.-H.; Yang, Z.-Y.; Hu, Q.-M. Synthesis, Structural Characterization, and Some Properties of New N-Functionally Substituted Diiron Azadithiolate Complexes as Biomimetic Models of Iron-Only Hydrogenases. *Organometallics* **2007**, *26*, 4921–4929.

(50) He, J.; Deng, C.-L.; Li, Y.; Li, Y.-L.; Wu, Y.; Zou, L.-K.; Mu, C.; Luo, Q.; Xie, B.; Wei, J.; Hu, J.-W.; Zhao, P.-H.; Zheng, W. A New Route to the Synthesis of Phosphine-Substituted Diiron Aza- and Oxadithiolate Complexes. *Organometallics* **2017**, *36*, 1322–1330.

(51) Chouffai, D.; Zampella, G.; Capon, J.-F.; De Gioia, L.; Gloaguen, F.; Pétillon, F. Y.; Schollhammer, P.; Talarmin, J. Oxidatively Induced Reactivity of [Fe₂(CO)₄(κ²-dppe)(μ-pdt)]: an Electrochemical and Theoretical Study of the Structure Change and Ligand Binding Processes. *Inorg. Chem.* **2011**, *50*, 12575–12585.

(52) Li, P.; Wang, M.; He, C.; Liu, X.; Jin, K.; Sun, L. Phosphane and Phosphite Unsymmetrically Disubstituted Diiron Complexes Related to the Fe-Only Hydrogenase Active Site. *Eur. J. Inorg. Chem.* **2007**, *2007*, 3718–3727.

(53) Structures found in CSD-5.41 August 2020: Groom, C. R.; Bruno, I. J.; Lightfoot, M. P.; Ward, S. C. The Cambridge Structural Database. *Acta Crystallogr.* **2016**, *B72*, 171–179.

(54) Cobley, C. J.; Pringle, P. G. Probing the bonding of phosphines and phosphites to platinum by NMR. Correlations of ¹J(PtP) and Hammett substituent constants for phosphites and phosphines coordinated to platinum(II) and platinum(0). *Inorg. Chim. Acta* **1997**, *265*, 107–115.

(55) Trzeciak, A. M.; Ziolkowski, J. J. Palladium Chemistry Related to Benzyl Bromide Carbonylation: Mechanistic Studies. *Monatsh. Chem.* **2000**, *131*, 1281–1291.

(56) Ahmad, N.; Ainscough, E. W.; James, T. A.; Robinson, S. D. Transition-metal complexes containing phosphorus ligands. Part IX. Triaryl phosphite derivatives of palladium(II) and platinum(II) dihalides. *J. Chem. Soc., Dalton Trans.* **1973**, 1148–1150.

(57) Bedford, R. B.; Betham, M.; Coles, S. J.; Horton, P. N.; López-Sáez, M.-J. The influence of steric bulk on the geometry of triarylphosphite-based palladacycles and their tricyclohexylphosphine adducts. *Polyhedron* **2006**, *25*, 1003–1010.

(58) Trzeciak, A. M.; Bartosz-Bechowski, H.; Ciunik, Z.; Niesyty, K.; Ziolkowski, J. J. Structural studies of PdCl₂L₂ complexes with fluorinated phosphines, phosphites, and phosphinites as precursors of benzyl bromide carbonylation catalysts, and and X-ray crystal structure of *cis*-PdCl₂[PPh₂(OEt)]₂. *Can. J. Chem.* **2001**, *79*, 752–759.

(59) Barton, B. E.; Rauchfuss, T. B. Terminal Hydride in [FeFe]-Hydrogenase Model Has Lower Potential for H₂ Production Than the Isomeric Bridging Hydride. *Inorg. Chem.* **2008**, *47*, 2261–2263.

(60) Eilers, G.; Schwartz, L.; Stein, M.; Zampella, G.; de Gioia, L.; Ott, S.; Lomoth, R. Ligand versus Metal Protonation of an Iron Hydrogenase Active Site Mimic. *Chem. - Eur. J.* **2007**, *13*, 7075–7084.

(61) Gao, S.; Fan, J.; Sun, S.; Peng, X.; Zhao, X.; Hou, J. Selenium-bridged diiron hexacarbonyl complexes as biomimetic models for the active site of Fe-Fe hydrogenases. *Dalton Trans.* **2008**, 2128–2135.

(62) Gloaguen, F.; Lawrence, J. D.; Schmidt, M.; Wilson, S. R.; Rauchfuss, T. B. Synthetic and Structural Studies on

- [Fe₂(SR)₂(CN)_x(CO)_{6-x}]^{x-} as Active Site Models for Fe-Only Hydrogenases. *J. Am. Chem. Soc.* **2001**, *123*, 12518–12527.
- (63) Mejia-Rodriguez, R.; Chong, D.; Reibenspies, J. H.; Soriaga, M. P.; Darensbourg, M. Y. The Hydrophilic Phosphatridazaadamantane Ligand in the Development of H₂ Production Electrocatalysts: Iron Hydrogenase Model Complexes. *J. Am. Chem. Soc.* **2004**, *126*, 12004–12014.
- (64) Rana, A.; Kumar Das, P.; Mondal, B.; Dey, S.; Crouthers, D.; Dey, A. Investigation of Bridgehead Effects on Reduction Potential in Alkyl and Aryl Azadithiolate-Bridged (μ -SCH₂XCH₂S) [Fe(CO)₃]₂ Synthetic Analogues of [FeFe]-H₂ase Active Site. *Eur. J. Inorg. Chem.* **2018**, *2018*, 3633–3643.
- (65) Si, G.; Wang, W.-G.; Wang, H.-Y.; Tung, C.-H.; Wu, L.-Z. Facile Synthesis and Functionality-Dependent Electrochemistry of Fe-Only Hydrogenase Mimics. *Inorg. Chem.* **2008**, *47*, 8101–8111.
- (66) Chong, D.; Georgakaki, I. P.; Mejia-Rodriguez, R.; Sanabria-Chinchilla, J.; Soriaga, M. P.; Darensbourg, M. Y. Electrocatalysis of hydrogen production by active site analogues of the iron hydrogenase enzyme: structure/function relationships. *Dalton Trans.* **2003**, 4158–4163.
- (67) Dey, S.; Rana, A.; Dey, S. G.; Dey, A. Electrochemical Hydrogen Production in Acidic Water by an Azadithiolate Bridged Synthetic Hydrogenase Mimic: Role of Aqueous Solvation in Lowering Overpotential. *ACS Catal.* **2013**, *3*, 429–436.
- (68) Hou, J.; Peng, X.; Liu, J.; Gao, Y.; Zhao, X.; Gao, S.; Han, K. A Binuclear Isocyanide Azadithiolatoiron Complex Relevant to the Active Site of Fe-Only Hydrogenases: Synthesis, Structure and Electrochemical Properties. *Eur. J. Inorg. Chem.* **2006**, *2006*, 4679–4686.
- (69) Song, L.-C.; Yang, Z.-Y.; Bian, H.-Z.; Liu, Y.; Wang, H.-T.; Liu, X.-F.; Hu, Q.-M. Diiron Oxadithiolate Type Models for the Active Site of Iron-Only Hydrogenases and Biomimetic Hydrogen Evolution Catalyzed by Fe₂(μ -SCH₂OCH₂S- μ)(CO)₆. *Organometallics* **2005**, *24*, 6126–6135.
- (70) Li, A.; Yang, J.; Lü, S.; Gui, M.-S.; Yan, P.; Gao, F.; Du, L.-B.; Yang, Q.; Li, Y.-L. Synthesis, characterization and electrochemical properties of diiron azadithiolate complexes Fe₂[(μ -SCH₂)₂NCH₂CCH](CO)₃L (L = CO or monophosphines). *Polyhedron* **2021**, *196*, 115007.
- (71) Chiarotto, I.; Carelli, I.; Carnicelli, V.; Marinelli, F.; Arcadi, A. Electrochemical behaviour of Pd^{II}(PPh₃)₂Cl₂ in the presence of carbon monoxide and its use in the palladium-catalyzed electrochemical formylation of iodoanisole. *Electrochim. Acta* **1996**, *41*, 2503–2509.
- (72) Downard, A. J.; Bond, A. M.; Clayton, A. J.; Hanton, L. R.; McMorran, D. A. Cyclic Voltammetry of Palladium(II) Complexes with Tridentate Arsine Ligands. Separation of the Two Single-Electron Transfer Steps of the Pd(II) - Pd(0) Interconversion Based on Thermodynamic and Kinetic Discrimination. *Inorg. Chem.* **1996**, *35*, 7684–7690.
- (73) The spectral window was open to –40 ppm in order to discard the presence of M–H species.
- (74) Davies, J. A.; Uma, V. A re-investigation of the electrochemistry of isomeric [PtCl₂(PR₃)₂] complexes by cyclic voltammetry. *Inorg. Chim. Acta* **1983**, *76*, L305–L307.
- (75) Davies, J. A.; Uma, V. An investigation of the isomerization reactions of [PtCl₂(PR₃)₂] complexes by cyclic voltammetry. *J. Electroanal. Chem. Interfacial Electrochem.* **1983**, *158*, 13–24.
- (76) Pozdeeva, A. A.; Tolstikov, G. A.; Chernova, V. A.; Zhdanov, S. I.; Dzhemilev, U. M. Electrochemical reduction of palladium (II) complexes with benzonitrile and organophosphorus ligands in an aprotic medium. *Bull. Acad. Sci. USSR, Div. Chem. Sci.* **1983**, *32*, 2022–2028.
- (77) Zhao, Y.; Truhlar, D. G. Density Functionals with Broad Applicability in Chemistry. *Acc. Chem. Res.* **2008**, *41*, 157–167.
- (78) Zhao, Y.; Truhlar, D. G. The M06 suite of density functionals for main group thermochemistry, thermochemical kinetics, non-covalent interactions, excited states, and transition elements: two new functionals and systematic testing of four M06-class functionals and 12 other functionals. *Theor. Chem. Acc.* **2008**, *120*, 215–241.
- (79) Zhao, Y.; Truhlar, D. G. Applications and validations of the Minnesota density functionals. *Chem. Phys. Lett.* **2011**, *502*, 1–13.
- (80) Wheeler, S. E.; Houk, K. N. Integration Grid Errors for Meta-GGA-Predicted Reaction Energies: Origin of Grid Errors for the M06 Suite of Functionals. *J. Chem. Theory Comput.* **2010**, *6*, 395–404.
- (81) Grimme, S.; Antony, J.; Ehrlich, S.; Krieg, H. A consistent and accurate ab initio parametrization of density functional dispersion correction (DFT-D) for the 94 elements H–Pu. *J. Chem. Phys.* **2010**, *132*, 154104.
- (82) Frisch, M. J.; Trucks, G. W.; Schlegel, H. B.; Scuseria, G. E.; Robb, M. A.; Cheeseman, J. R.; Scalmani, G.; Barone, V.; Petersson, G. A.; Nakatsuji, H.; Li, X.; Caricato, M.; Marenich, A. V.; Bloino, J.; Janesko, B. G.; Gomperts, R.; Mennucci, B.; Hratchian, H. P.; Ortiz, J. V.; Izmaylov, A. F.; Sonnenberg, J. L.; Williams, D.; Ding, F.; Lipparini, F.; Egidi, F.; Goings, J.; Peng, B.; Petrone, A.; Henderson, T.; Ranasinghe, D.; Zakrzewski, V. G.; Gao, J.; Rega, N.; Zheng, G.; Liang, W.; Hada, M.; Ehara, M.; Toyota, K.; Fukuda, R.; Hasegawa, J.; Ishida, M.; Nakajima, T.; Honda, Y.; Kitao, O.; Nakai, H.; Vreven, T.; Throssell, K.; Montgomery, Jr., J. A.; Peralta, J. E.; Ogliaro, F.; Bearpark, M. J.; Heyd, J. J.; Brothers, E. N.; Kudin, K. N.; Staroverov, V. N.; Keith, T. A.; Kobayashi, R.; Normand, J.; Raghavachari, K.; Rendell, A. P.; Burant, J. C.; Iyengar, S. S.; Tomasi, J.; Cossi, M.; Millam, J. M.; Klene, M.; Adamo, C.; Cammi, R.; Ochterski, J. W.; Martin, R. L.; Morokuma, K.; Farkas, O.; Foresman, J. B.; Fox, D. J. *Gaussian 16*, rev. C.01; Gaussian, Inc.: Wallingford, CT, 2016.
- (83) Andrae, D.; Häußermann, U.; Dolg, M.; Stoll, H.; Preuß, H. Energy-adjusted ab initio pseudopotentials for the second and third row transition elements. *Theor. Chim. Acta* **1990**, *77*, 123–141.
- (84) Ehlers, A. W.; Böhme, M.; Dapprich, S.; Gobbi, A.; Höllwarth, A.; Jonas, V.; Köhler, K. F.; Stegmann, R.; Veldkamp, A.; Frenking, G. A set of f-polarization functions for pseudo-potential basis sets of the transition metals Sc–Cu, Y–Ag and La–Au. *Chem. Phys. Lett.* **1993**, *208*, 111–114.
- (85) Hehre, W. J.; Ditchfield, R.; Pople, J. A. Self-Consistent Molecular Orbital Methods. XII. Further Extensions of Gaussian-Type Basis Sets for Use in Molecular Orbital Studies of Organic Molecules. *J. Chem. Phys.* **1972**, *56*, 2257–2261.
- (86) Francel, M. M.; Pietro, W. J.; Hehre, W. J.; Binkley, J. S.; Gordon, M. S.; DeFrees, D. J.; Pople, J. A. Self-consistent molecular orbital methods. XXIII. A polarization-type basis set for second-row elements. *J. Chem. Phys.* **1982**, *77*, 3654–3665.
- (87) Marenich, A. V.; Cramer, C. J.; Truhlar, D. G. Universal Solvation Model Based on Solute Electron Density and on a Continuum Model of the Solvent Defined by the Bulk Dielectric Constant and Atomic Surface Tensions. *J. Phys. Chem. B* **2009**, *113*, 6378–6396.